DOI: 10.61782/fa.2023.0703

forum acusticum 2023

STABILITY LIMITS OF AN ELECTROACOUSTIC ABSORBER

Maxime Volery[1] **Hervé Lissek**[1*]
[1] Acoustic Group - Signal Processing Laboratory LTS2, EPFL, Lausanne, Switzerland

ABSTRACT

Active sound absorption can be achieved by the digital control of an electrodynamic loudspeaker. So far, the stability limits of these absorbers were only empirically estimated for each acoustic environment. This work presents how it is possible to use the controller of the absorber to measure the acoustic environment, and how it can be used to predict its stability limits. It is also shown how these stability limits can be exploited to optimize the controller to obtain the most stable system.

Keywords: *active sound absorption, stability margins, electrodynamic loudspeaker*

1. INTRODUCTION

Active electroacoustic absorption consists in turning a loudspeaker into a sound absorber by actively modifying the acoustic impedance presented by its membrane. Typically, the current driving the loudspeaker is calculated in real-time from different measured quantities of the absorber (e.g., pressure in front and/or behind the membrane) allowing tailoring the response from the front pressure to the membrane velocity to meet the desired behavior [1]. However, if the desired behavior is too much different from the passive case (e.g., increasing the resonance frequency by more than two or three times), the system is likely to be unstable [2]. The main reasons for these instabilities are inaccuracies in the model of the loudspeaker, typically a poor estimation of the parameters, or a too large input-output latency of the controller. This work presents how measuring the inputs of the controller when an arbitrary broadband current is driving the absorber enables the designer to gain some knowledge about the acoustic environment, allowing them to calculate the stability margins of the system, and to predict if a given target is achievable or unstable. Furthermore, the stability margins calculation can help in choosing the optimal control strategy for a given target.

**Corresponding author*: *herve.lissek@epfl.ch.*

2. MODEL OF THE ACTUATOR

This section presents the analytical model of the loudspeaker that is required by the controller. An electrodynamic loudspeaker is a second-order mass-spring-damper resonator with mass M_{ss}, compliance C_{ms} and mechanical resistance R_{ms} [3]. Three forces are acting on its membrane: pressure in front p_f and behind p_b the membrane and the Lorentz force created by the current i flowing in the voice coil. When mounted on an enclosure, the rear pressure contribution can be linked to the membrane displacement by the specific compliance of the cabinet which is the ratio between the membrane displacement and the pressure in the cavity, and it is proportionally related to the volume of air enclosed in the cavity V_b

$$C_{sb} = V_b(\rho c^2 S_d)^{-1}, \tag{1}$$

where ρ is the mass density of the air, c speed of sound in the air, and S_d is the effective piston area of the loudspeaker. The motion of the membrane is then found by Newton's second law of motion. In the Laplace domain, with Laplace variable s, the model of the loudspeaker is

$$\begin{cases} p_f(s) = Z_{sc}(s)v(s) + Fi(s) \\ p_b(s) = v(s)/\left(sC_{sb}\right) \end{cases}, \tag{2}$$

where $F = Bl/S_d$,

$$Z_{sc}(s) = sM_{ss} + R_{ss} + \frac{1}{s}\underbrace{\left(\frac{1}{S_d C_{ms}} + \frac{1}{C_{sb}}\right)}_{1/C_{sc}}, \tag{3}$$

is the specific impedance of the loudspeaker mounted on the cabinet, $M_{ss} = M_{ms}/S_d$ is the specific moving

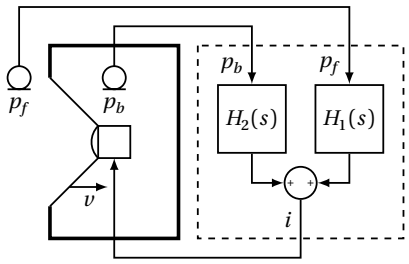

Figure 1. Controlled absorber

mass of the speaker, $R_{ss} = R_{ms}/S_d$ its specific resistance, C_{sc} the combined specific compliance of the speaker and the enclosure. The angular resonance frequency of the absorber is $\omega_0 = 1/\sqrt{M_{ss}C_{sc}}$ and its quality factor $Q = R_{ss}^{-1}\sqrt{M_{ss}/C_{sc}}$.

Because an accurate model of the electrical impedance of the inductance of the voice coil is complex to develop and estimate [4] and because the force acting on the membrane is proportional to the current, it is good to control the current flowing in the coil rather than its voltage. A voltage-controlled current source can for instance be realized using a Howland current pump [5].

3. MIXED FEEDFORWARD-FEEDBACK CONTROLLER

The controller used for the absorber realization consists in acquiring the front and rear pressures p_f and p_b with microphones connected to a field-programmable gate array (FPGA) which calculates in real-time the appropriate current to inject in the loudspeaker [2]

$$i = H_1(s)p_f + H_2(s)p_b, \tag{4}$$

where both $H_1(s)$ and $H_2(s)$ are digital filters implemented on the FPGA. These control transfer functions are

$$H_1(s) = \frac{1}{F}\left(1 - \frac{Z_{sc}(s) + G(s)}{Z_{st}(s)}\right) \tag{5}$$

$$H_2(s) = \frac{sC_{sb}G(s)}{F}, \tag{6}$$

where Z_{st} is the specific target impedance and $G(s)$ is a first order low-pass filter with gain k_g and cutoff angular frequency ω_g. An illustration of this controller is shown in figure 1.

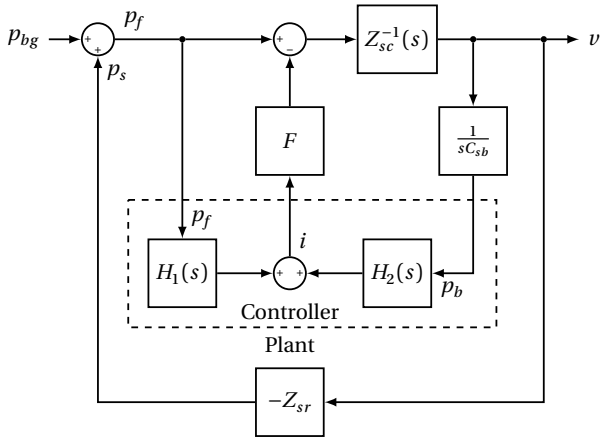

Figure 2. Block diagram of the absorber in its acoustic environment (controller is in the dashed rectangle)

4. STABILITY MARGINS

In practice, this absorber is placed in an acoustic environment which will create a feedback loop on the absorber through its specific radiation impedance $Z_{sr}(s)$. A block diagram of the absorber in the acoustic environment is shown in figure 2, in which two feedback loops are identifiable. The internal one is from the controller and serves to improve its robustness. The second one is due to the radiation impedance from the absorber: its moving membrane will create a scattered pressure field p_s in front of it, and the total pressure is the sum of this scattered field and the background field p_{bg}, which is the total field when the membrane does not move at all

$$p_f = p_{bg} + p_s = p_{bg} - Z_{sr}(s)v. \tag{7}$$

Note that the negative sign in the radiation impedance is due to the direction in which the membrane velocity is defined. The controller $\mathbf{H}(s) = \begin{bmatrix} H_1(s) & H_2(s) \end{bmatrix} \in \mathbb{C}^{1\times 2}$ is visible in the dashed rectangle. Everything else is the plant $\mathbf{P}(s) = \begin{bmatrix} \mathbf{P}_1(s)\mathbf{P}_2(s) \end{bmatrix} \in \mathbb{C}^{2\times 2}$

$$\begin{bmatrix} p_f \\ p_b \end{bmatrix} = \underbrace{\frac{1}{Z_{sc} + Z_{sr}} \begin{bmatrix} FZ_{sr} & Z_{sc} \\ -F/(sC_{sb}) & (sC_sb)^{-1} \end{bmatrix}}_{\mathbf{P}(s)} \begin{bmatrix} i \\ p_{bg} \end{bmatrix}. \tag{8}$$

The description of the system as a combination of a plant and controller transfer functions is shown in figure 3 in the negative feedback loop appears evident.

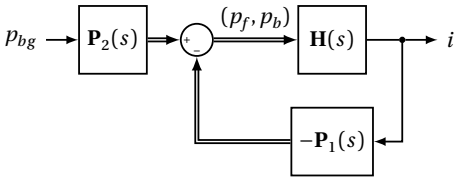

Figure 3. Block diagram of the plant and the controller

Table 1. Parameters of the absorber

Parameter	Value
R_{ss}	$551.4\,\mathrm{Pa\,s\,m^{-1}}$
F	$498.3\,\mathrm{Pa\,A^{-1}}$
Q_{ms}	5.351
$w_0/(2\pi)$	482.4 Hz
C_{sb}	$0.8000\,\mathrm{\mu m\,Pa^{-1}}$

Because the frequency response of the radiation impedance $Z_{sr}(s)$ can be of a very complicated shape (environment dependent) and closed-form analytical solutions only exist in very specific cases, it is not feasible to analyze the stability of this loop from the location of its poles. It is nevertheless quite straightforward to measure the plant response by driving the output of the controller with an arbitrary broadband signal (e.g., white noise) and recording its two input signals. A bode plot of the measured plant response $\mathbf{P}_1(s)$ with the FPGA controller is shown in figure 4. The open loop transfer function is

$$\begin{aligned} T(s) &= -\mathbf{H}(s)\mathbf{P}_1(s) \\ &= \frac{-F}{Z_{sc}+Z_{sr}}\left(H_1 Z_{sr} - \frac{H_2}{sC_{sb}}\right), \end{aligned} \tag{9}$$

which is possible to evaluate with an analytical frequency response of the controller. For the transducer parameters of table 1 and

$$Z_{st}(s) = R_{st}\frac{s^2 + s\omega_t/Q_t + \omega_t^2}{s\omega_t/Q_t} \tag{10}$$

with $R_{st} = \rho c$, $Q_t = 7$, $\omega_t = 2\pi \cdot 1\,\mathrm{kHz}$ the obtained open-loop response is shown for a control with $k_g = 0$ (feedforward only) and with $k_g = 4.2$ and $\omega_g = 2\pi \cdot 1.5\,\mathrm{kHz}$ (with feedback) in the Nyquist plot of figure 5, in which the frequency response of $T(s)$ is plotted in the complex pane.

The Nyquist plot enables the determination of the stability of the closed loop with negative feedback [6].

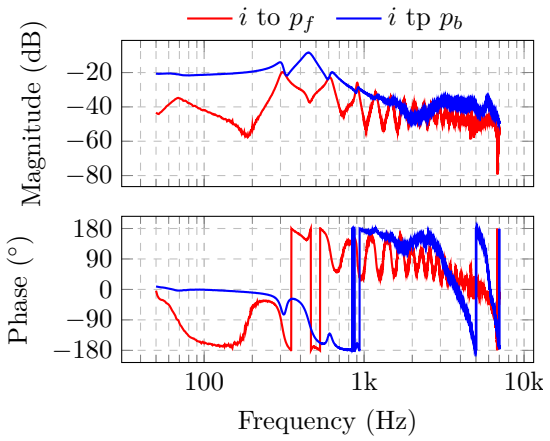

Figure 4. Measured frequency response of the plant $\mathbf{P}_1(s)$ in a slightly damped duct (from the controller output voltage to its input voltages)

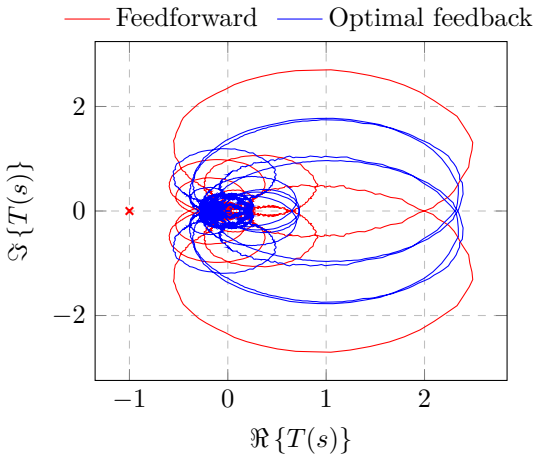

Figure 5. Nyquist plot of the feedforward and $k_g = 4.2$, $\omega_g = 2\pi \cdot 1.5\,\mathrm{kHz}$ open loops

The Nyquist theorem states that for stable open loops, the closed loop is stable if and only if the Nyquist contour does not cross the real axis at values smaller or equal to -1. Furthermore, from this plot, it is possible to define the stability margins. The gain and phase margins G_m and ϕ_m are the amount of gain/phase that can be introduced in the open loop before the closed loop gets unstable. Another metric that combines both gain and phase margin information is the disk margin D_m [7]. It is the smallest distance d (across all frequencies) from the Nyquist curve to the

Table 2. Predicted stability margins

Margin	Feedforward	Optimal feedback
G_m	7.99 dB (341 Hz)	10.35 dB (585 Hz)
ϕ_m	$-60.8°$ (874 Hz)	$57.8°$ (1.02 kHz)
D_m	0.517 (51.6 Hz)	0.643 (92.0 Hz)

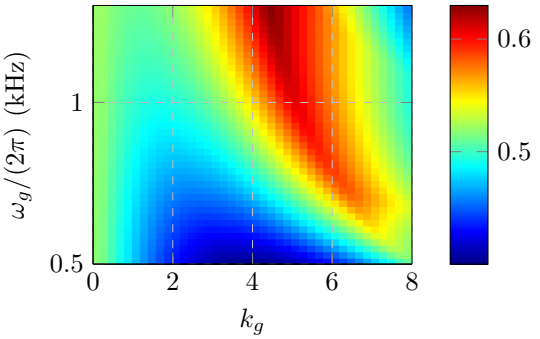

Figure 6. Disk margins of different feedback settings

critical point $-1+0j$

$$D_m = \min_{\omega} |T(j\omega)+1| . \tag{11}$$

The evaluation of these margins and the frequencies at which they occur are reported in table 2

5. OPTIMAL PARAMETERS OF THE FEEDBACK

To find the optimal control parameters k_g and ω_g, the disk margin is evaluated for each possible combination of parameters. The result of this sweep is shown in figure 6, in which the cutoff frequency is restricted to the range $0.5\,\mathrm{kHz}$ to $1.5\,\mathrm{kHz}$. The lower limit of the range has been selected around the resonance frequency of the loudspeaker, and the upper boundary at $1.5\,\mathrm{kHz}$ because it corresponds to a quarter wavelength of $\lambda/4 = 57\,\mathrm{mm}$ and the box dimensions are of the same order of magnitude ($V_b^{1/3} = 38\,\mathrm{mm}$). In this figure, the optimal values (largest disk margin) are $k_g = 4.2$ and $\omega_g = 2\pi \cdot 1.5\,\mathrm{kHz}$. It is noticeable in figure 5 that the contribution of the feedback $G(s)$ helps to improve the stability and shifts the Nyquist curve further away from $-1+0j$.

6. CONCLUSION

Thanks to the digital nature of the controller, it is possible to estimate the plant response and assess the stability of a given target impedance for direct impedance control. It has been shown in this work that the forward architecture can be made more robust by introducing a feedback contribution. The predicted stability margins could also be used to estimate at which frequency the instability of a too-extreme target impedance will most likely occur. The knowledge of the plant response can be further exploited to calculate the region of target impedance parameters that are stable and their corresponding optimal controller.

7. ACKNOWLEDGMENT

This project has received funding from the Clean Sky 2 Joint Undertaking under the European Union's Horizon 2020 research and innovation program under grant agreement No 821093. This publication reflects only the authors' view, and the JU is not responsible for any use that may be made of the information it contains.

8. REFERENCES

[1] E. Rivet, S. Karkar, and H. Lissek, "Broadband low-frequency electroacoustic absorbers through hybrid sensor-/shunt-based impedance control," *IEEE Transactions on Control Systems Technology*, vol. 25, no. 1, 2017.

[2] M. Volery, X. Guo, and H. Lissek, "Robust direct acoustic impedance control using two microphones for mixed feedforward-feedback controller," *Acta Acust.*, vol. 7, 2023.

[3] M. Rossi, *Audio*. Presses Polytechniques et Universitaires Romandes, 2007.

[4] W. M. Leach Jr., "Loudspeaker voice-coil inductance losses: Circuit models, parameter estimation, and effect on frequency response," *Journal of the Audio Engineering Society*, vol. 50, no. 6, Jun. 2002.

[5] *A comprehensive study of the Howland current pump*, AN-1515, Application report, Texas Instruments, Jan. 2008. [Online]. Available: `https://www.ti.com/lit/an/snoa474a/snoa474a.pdf`.

[6] C. E. Rohrs, "The circuits and filters handbook," in W.-K. Chen, Ed. CRC-Press, 1995, ch. The Nyquist criterion.

[7] P. Seiler, A. Packard, and P. Gahinet, "An introduction to disk margins," *IEEE Control Systems Magazine*, vol. 40, no. 5, 2020.